

pubs.acs.org/JPCA Article

Electronic Spectroscopy and Photoionization of LiMg

Published as part of The Journal of Physical Chemistry virtual special issue "Alexander Boldyrev Festschrift". Thomas D. Persinger, Jiande Han, and Michael C. Heaven*



Cite This: https://doi.org/10.1021/acs.jpca.1c01656

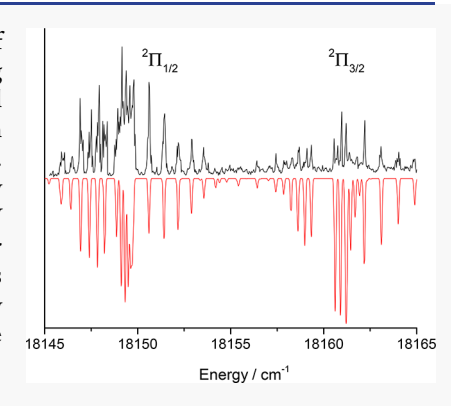


ACCESS

Metrics & More

Article Recommendations

ABSTRACT: Dimers consisting of an alkali metal bound to an alkaline earth metal are of interest from the perspectives of their bonding characteristics and their potential for being laser cooled to ultracold temperatures. There have been experimental and theoretical studies of many of these species, but spectroscopic data for LiMg and the LiMg⁺ cation are sparse. In this study, rotationally resolved electronic spectra for LiMg are presented. The ground state is confirmed to be $X1^2\Sigma^+$ and observations of low-lying electronically excited states are reported for the first time. Reexamination of transitions in the near-UV spectral range indicates that previous band assignments should be revised. Two-color laser excitation techniques were used to determine an ionization energy of 4.7695(4) eV. This value is 1.2 eV below the previously reported experimental estimate. Vibrationally resolved spectra were obtained for LiMg⁺, yielding molecular constants that were consistent with a substantial strengthening of the bond on ionization.



INTRODUCTION

Interest in metal dimers that consist of an alkali atom bound to an alkaline earth atom (Alk-AE) was originally motivated by questions concerning the strength and the mechanisms of bonding. $^{1-7}$ For example, Bauschlicher et al. 1 considered the question of whether the bonding would be intermediate between the covalent bonds of the Alk-Alk dimers and the van der Waals-like bonding of the AE-AE dimers. Over the past decade there has been additional interest in the Alk-AE dimers generated by the possibility that they may be suitable for cooling to ultracold temperatures. An ensemble of these dimers would be able to process information by means of both electric dipole and spin—spin interactions. Molecular ions of the form Alk-AE+ have closed shell $^1\Sigma^+$ ground states. While they do not offer the advantages of facilitating magnetic interactions through spin, they can be trapped and manipulated using external electric fields.

There have been many theoretical and experimental studies of the Alk-AE dimers. $^{1-15,21,24-50}$ As the present study is focused on LiMg, we briefly summarize the gas-phase spectroscopic work that has been carried out on the Li-AE series. Electronic spectra have been recorded for LiBe, LiMg, 5,38 LiCa, 6,47,48 LiSr, 45,49,50 and LiBa. 29,40 With the exception of LiMg, a subset of the spectra for each dimer has been recorded at the level of rotational resolution. All of the dimers have $X1^2\Sigma^+$ ground states. The first excited states are $1^2\Pi$ and $2^2\Sigma^+$, which correlate with the Li(2p) + AE(ns^2) dissociation asymptote. These bound states are all less than 11000 cm $^{-1}$ above the ground states minimum for the entire series. The next group of excited states, $2^2\Pi$, $3^2\Sigma^+$, $1^4\Pi$, and

 $1^4\Sigma^+$, correlate with the Li(2s) + AE(nsnp, 3 P) atomic limit. The ground state dissociation energies do not vary monotonically with the increasing atomic number of AE, with LiMg having the weakest bond.²

The lightest member of this family, LiBe, was characterized by means of laser-induced fluorescence (LIF) spectroscopy. Schlachta et al.4 observed rotationally resolved bands of the $2^{2}\Pi$ -X1² Σ ⁺ transition within the range 19200–20600 cm⁻¹. Multireference configuration interaction (MRCI) calculations predicted that the ground state was bound by 2476 cm⁻¹ consistent with the expected half-order bond. The bond length was found to be shorter than that of covalently bound Li₂, in part due to the smaller covalent radius of Be. Electronic spectra for ⁷Li²⁴Mg, recorded by means of resonantly enhanced two-photon ionization (RE2PI), were reported by Berry and Duncan. Two electronic band systems labeled E-X1 $^2\Sigma^+$ and F- $X1^{2}\Sigma^{+}$ were observed in the 30000-32000 cm⁻¹ range. Data were taken at the level of vibrational resolution. Hot bands were observed, allowing for determination of the ground state binding energy ($D_0 = 1330 \text{ cm}^{-1}$) via extrapolation of the vibrational structure. The E and F states were tentatively assigned as the ${}^{2}\Pi$ and ${}^{2}\Sigma^{+}$ states correlating with the Li(3p) + $Mg(3s^2)$ dissociation asymptote. Bound-free emission spectra

Received: February 23, 2021 Revised: April 8, 2021



for the lower energy $2^2\Pi - X1^2\Sigma^+$ and $3^2\Sigma^+ - X1^2\Sigma^+$ transitions of LiMg were reported by Pichler et al.³⁸ The emissions were generated by the reaction of optically excited Li₂ with Mg atoms.

There have been several theoretical calculations for LiMg. Ground state properties are discussed in refs 2, 3, 8–11, and 38. Two of the more recent studies have examined the $\rm X1^2\Sigma^+$ state rotation-vibration transition rates associated with ambient temperature blackbody radiation. Electronically excited states up to those correlating with the Li(2s) + Mg(3s3p, 3P) asymptotes were explored in refs 10 and 38. Table 1 lists the atomic state asymptotes and the molecular terms that correlate with these limits for states that are relevant to this study.

Table 1. Correlation of Molecular Electronic States of LiMg with Separated Atom Limits

Li	Mg	$E(Li)^a$	$E(Mg)^a$	total energy	molecular terms
2s	$3s^2$	0.0	0.0	0.0	$X1^2\Sigma^+$
2p	$3s^2$	14903.8	0.0	14903.8	$2^{2}\Sigma^{+}$, $1^{2}\Pi$
2s	3s3p(³ P)	0.0	21890.9	21890.9	$3^{2}\Sigma^{+}$, $2^{2}\Pi$, $1^{4}\Sigma^{+}$, $1^{4}\Pi$
3s	$3s^2$	27206.1	0.0	27206.1	$4^2\Sigma^+$
3p	$3s^2$	30925.4	0.0	30925.4	$5^{2}\Sigma^{+}$, $3^{2}\Pi$
3d	$3s^2$	31283.1	0.0	31283.1	$6^{2}\Sigma^{+}$, $4^{2}\Pi$, $1^{2}\Delta$
4s	$3s^2$	35012.1	0.0	35012.1	$7^2\Sigma^+$
2s	$3s3p(^{1}P)$	0.0	35051.3	35051.3	$8^2\Sigma^+$, $5^2\Pi$
2p	3s3p(³ P)	14903.8	21890.9	36794.7	$9^{2}\Sigma^{+}$, $10^{2}\Sigma^{+}$, $1^{2}\Sigma^{-}$, $6^{2}\Pi$, $7^{2}\Pi$, $2^{2}\Delta$, $2^{4}\Sigma^{+}$, $3^{4}\Sigma^{+}$, $1^{4}\Sigma^{-}$, $2^{4}\Pi$, $3^{4}\Pi$, $1^{4}\Delta$

^aEnergies from the NIST atomic database⁵⁷ in units of cm⁻¹.

The objectives of the present study were to advance the characterization of LiMg by recording rotationally resolved spectra for the near-UV bands reported by Berry and Duncan and provide the first observations of the lower energy $1^2\Pi$, $2^2\Sigma^+$, $2^2\Pi$ and $3^2\Sigma^+$ states. This was accomplished by means of LIF, dispersed fluorescence, and RE2PI measurements. Fluorescence decay lifetimes were recorded in order to test transition dipole moment predictions for several excited state. To examine the configurational parentage of the states observed in the near-UV spectral range, we have carried out MRCI calculations that now include states that correlate with the Li(nl) + Mg($3s^2$), limits for nl = 3s, 3p, 3d, and 4s.

The ionization energy (IE) of LiMg and the ground state vibrational structure of LiMg⁺ were probed by means of pulsed-field ionization zero-kinetic energy (PFI-ZEKE) photoelectron spectroscopy.⁵¹ The IE was in question as an early measurement carried out using mass spectrometry yielded a value of 5.96 eV. Subsequently, spectroscopic measurements 5 and theoretical calculations² indicated that this value was too high by at least 1 eV. Prior to the present study there were no published spectroscopic studies of the ion, but calculated properties for LiMg⁺ were available from refs 2, 10, 16, and 52. The most recent study 52 predicts a $X1^{1}\Sigma^{+}$ ground state dissociation energy of 6575 cm⁻¹, with vibrational and rotational constants of $\omega_e^+ = 264$ and $B_e^+ = 0.372$ cm⁻¹. The lifetimes of the ground state vibrational levels in the presence of blackbody radiation have been considered by Gao and Gao¹⁰ and Fedorov et al.,⁵² while properties of low-lying electronically excited states have been investigated by Gao and Gao¹⁰ and ElOualhazi et al.¹⁶

EXPERIMENTAL SECTION

The techniques used to characterize LiMg consisted of LIF, dispersed LIF (DLIF), RE2PI, photoionization efficiency (PIE), and PFI-ZEKE spectroscopy. Gas-phase LiMg was obtained by laser ablation of the surface of a Li-coated Mg rod (as in the study by Berry and Duncan⁵). The Li coating was applied by rubbing samples of Li metal against the surface of the 6.35 mm diameter Mg rod. Laser ablation was achieved using the 1064 nm pulses from a Nd/YAG laser. Typically, the rod could be used for about 3 days before the Li coating needed to be reapplied.

The Li-coated Mg rod was mounted in a Smalley-type jet expansion source. 53 The rod was rotated and translated to avoid pitting. The carrier gas used for these experiments was pure He, supplied by a pulsed valve (Parker-Hannifin series 9) at a source pressure of 5 atm. LIF and DLIF spectra were recorded with the excitation laser beam set to cross the jet expansion approximately 7.5 cm downstream from the nozzle orifice. Laser-induced fluorescence was collected along an axis that was perpendicular to both the laser beam axis and the jet expansion axis. For the recording of LIF data, a long-pass filter was used to reduce the scattered laser light, and the filtered fluorescence was detected by a photomultiplier tube (Photonis XP2020). Fluorescence decay curves, acquired using a digital oscilloscope (LeCroy WaveSurfer 24Xs) to signal-average 500 laser pulses per trace, were measured using the same setup. DLIF spectra were obtained when the long-pass filter was replaced by a 0.25 m monochromator (Jarrell-Ash 82-410).

Three tunable dye laser systems were used in these experiments. Two were Nd/YAG pumped systems, consisting of a Lambda Physik Scan Mate Pro driven by a Quantel Qsmart 850 Nd/YAG, and a Continuum ND6000 dye laser driven by a Powerlite 8000 Nd/YAG laser. The third system was a Lambda Physik FL3002 dye laser pumped by a Lextra XeCl excimer laser. In their standard configurations, all three dye lasers operated with line widths (FWHM) of approximately 0.3 cm⁻¹. For higher resolution measurements, the line width of the FL3002 laser was reduced to 0.06 cm⁻¹ by means of an intracavity etalon. Wavelength calibration of the lasers was established using a Bristol Instruments model 821 wave meter.

RE2PI, PIE, and PFI-ZEKE measurements were carried out in a differentially pumped vacuum chamber that was equipped for time-of-flight mass spectrometry and electron detection.⁵⁴ RE2PI and PIE spectra were recorded with mass-resolved ion detection. RE2PI data for the near-UV bands were obtained using one-color, two-photon ionization. This was possible because the excited state energies were more than half of the IE. RE2PI spectra for lower energy states were observed using two-color ionization. Frequency doubling of the light from the ND6000 laser yielded wavelengths (usually near 330 nm and held constant for each scan) that could readily ionize LiMg that had been excited to the $2^2\Pi$ or $3^2\Sigma^+$ states. All two-color measurements were carried out using spatially overlapped, counter-propagating laser beams. Digital delay generators (Stanford Research Systems, DG 535) were used to synchronize the light pulses.

PIE curves were recorded with the first laser set to populate an excited state of LiMg. The wavelength of the second laser was then swept to locate the onset of ionization. These measurements were conducted with the ionization zone located between the charged electrodes of the mass

spectrometer. The local electric field of 364 V cm⁻¹ caused a depression of the IE by 115 cm⁻¹.

PFI-ZEKE spectra for LiMg⁺ were recorded with sequential laser excitation occurring under nominally field-free conditions. Sequential excitation to long-lived Rydberg states was followed by the application of a $1.4~\rm V~cm^{-1}$ pulse to induce field ionization and acceleration of the electrons to a microchannel plate detector. The delay between the laser excitation and ionizing field pulses was $2~\mu s$.

RESULTS

i. $2^2\Pi - X1^2\Sigma$ ⁺ and $3^2\Sigma$ ⁺ $-X1^2\Sigma$ ⁺ Transitions of LiMg.

The ab initio predictions of Gao and Gao¹⁰ were used to guide searches for the $2^2\Pi - X1^2\Sigma^+$ and $3^2\Sigma^+ - X1^2\Sigma^+$ transitions. Initially, RE2PI spectroscopy with mass-resolved ion detection was used to find the vibronic bands. This ensured that the observed features were associated with LiMg. Once the band centers had been located, LIF spectra were recorded as this technique yielded better resolution in the apparatus used for these measurements. Figure 1 shows a rotationally resolved

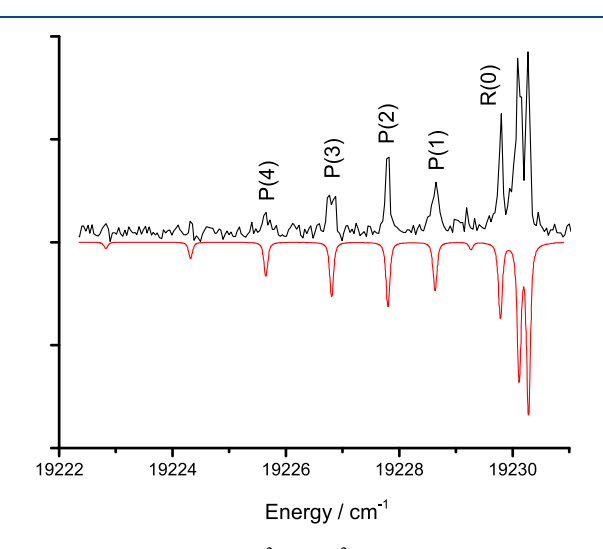


Figure 1. Origin band of the $3^2\Sigma^+-X1^2\Sigma^+$ transition. The downward-going (red) trace is a simulation generated using the PGOPHER software package. The peaks are labeled using the Hund's case (b) rotational quantum number N. The rotational temperature for this model was 5 K.

LIF spectrum for the origin band of the $3^2\Sigma^+-X1^2\Sigma^+$ transition, recorded using etalon line-narrowing to improve the line-width of the dye laser. This trace exhibits the expected P- and R-branch structure, but the resolution was not sufficient to expose either the spin-rotation or isotope splittings (the dominant isotopologues are ⁷Li²⁴ Mg (73%), ⁷Li²⁵ Mg (9%), and ⁷Li²⁶ Mg (10%)). The downward-going trace in Figure 1 is a simulation generated using the PGOPHER software package. 55 Due to the limited resolution and the small number of rotational levels observed, only three molecular constants could be derived for this band. These were the band origin (ν_0 = 19229.3 cm⁻¹) and the upper and lower state rotational constants (B_0') and B_0''). The band origin was just 140 cm⁻¹ below the value predicted at the MRCI/CVQZ+Q level of theory. 10 Also, in accord with the predictions, the rotational constant for the excited state $(0.248(2) \text{ cm}^{-1})$ was appreciably smaller than that of the ground state $(0.320(2) \text{ cm}^{-1})$,

reflecting an increase in the equilibrium bond length on excitation to the $3^2\Sigma^+$ state.

Rotationally resolved bands for the $3^2\Sigma^+-X1^2\Sigma^+$ transition were recorded for v'-v'' bands with v' = 0–7. The first cycle of constant fitting was carried out without the assumption of v'' = 0, such that ν_0 , B_0' and B_0'' were treated as independent variables. It was evident from the results that all of the bands originated from the ground state zero-point level. Consequently, the data were reanalyzed with B_0'' held constant at the average value obtained from the three-parameter fits ($B_0'' = 0.320 \text{ cm}^{-1}$). The final band origins and rotational constants for the $3^2\Sigma^+-X1^2\Sigma^+$ transition are listed in Table 2. The

Table 2. Molecular Constants for the $2^2\Pi - X1^2\Sigma^+$ and $3^2\Sigma^+ - X1^2\Sigma^+$ Transitions of LiMg^a

(i)	$2^2\Pi$ -X1 $^2\Sigma$ +				
v'	ν_0	В′	A'_{SO}		
0	18154.3	0.306(2)	12.0(1)		
1	18337.5	0.302(2)	12.7(1)		
2	18517.6	0.311(4)	13.3(2)		
(ii)		$3^2\Sigma^+$ – X	$1^2\Sigma^+$		
v'		ν_0	B'		
0	1	9229.3	0.248(2)		
1	19	9393.1	0.236(1)		
2	19	9554.8	0.232(2)		
3	19	9715.5	0.231(2)		
4	19	9875.1	0.227(1)		
5	20	0032.7	0.240(4)		
6	20	0183.9	0.239(4)		
7	20342.1		0.216(2)		

 $^{a}v_{0}$ and B' are given in units of cm⁻¹. $B''_{0} = 0.320(2)$ cm⁻¹. The 1σ error of the band origins was 0.1 cm⁻¹. The 1σ errors of the last digit for the rotational constants are given in parentheses.

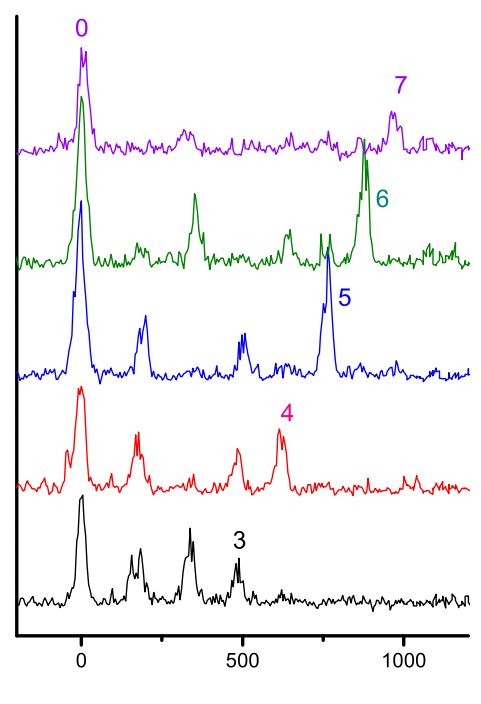
vibrational intervals were well-represented by the Morse energy level expression

$$E_{\text{vib}}(\mathbf{v}') = \omega_e'(\mathbf{v}' + 1/2) - \omega_e x_e'(\mathbf{v}' + 1/2)^2$$
 (1)

Fitting to this expression yielded vibrational constants of ω'_{ϵ} = 165.4(6) and $\omega_{\epsilon}x'_{\epsilon}$ = 0.83(9) cm⁻¹.

The increase in the equilibrium distance on excitation to the $3^2\Sigma^+$ state facilitated the observation of vibrational progressions in both the excitation and dispersed fluorescence spectra. Figure 2 shows a series of DLIF spectra recorded using excitation of the v'=0-4 upper states. These data have been plotted with the laser excitation energy set to 0 cm⁻¹, so that the ground state vibrational energies are vertically aligned. Note that the intensities of the E=0 cm⁻¹ features are artificially high due to the presence of scattered laser light. Due to the short fluorescence lifetime, we could not use time-gating to bias against the scattered light. However, the intensity contours of the nonresonant emission features confirmed the upper state vibrational quantum number assignments given in Table 2. Fluorescence decay lifetimes for the v'=0 and 1 levels were both 30 ns.

Band centers for the DLIF spectra, spanning the range v'' = 0-9, were determined by fitting Gaussian functions to the emission peaks. The vibrational energies relative to v'' = 0 are given in Table 3. At the level of resolution achieved, the vibrational energies were consistent with eq 1. Least squares fitting yielded ground state constants of $\omega''_{\varepsilon} = 187.3(16)$ and



Relative Energy /cm⁻¹

Figure 2. DLIF spectra recorded using excitation of the $3^2\Sigma^+$ – $X1^2\Sigma^+$ transition. The traces, in ascending order, were produced by excitation of the upper state levels v'=0, 1, 2, 3, and 4. Selected peaks are labeled by the lower state vibrational level on which the emission band terminates. See text for details.

Table 3. Ground State Vibrational Energies for LiMg and $LiMg^+$

v	LiMg $E(v)^a/cm^{-1}$	$LiMg^+ E(v)^b/cm^{-1}$
0	0	0
1	177	264
2	331	520
3	486	773
4	628	1027
5	751	1269
6	876	1508
7	959	1742
8	1053	1969
9	1132	2195

 $^{^{}a}1\sigma$ error of 6 cm⁻¹. $^{b}1\sigma$ error of 3 cm⁻¹.

 $\omega_e x_e'' = 6.16(19) \text{ cm}^{-1}$. The standard deviation for this fit was 5.8 cm⁻¹. Application of the Morse expression for the dissociation energy $(D_e = (\omega_e^2/4\omega_e x_e))$ gave a value of $1424(21) \text{ cm}^{-1}$.

The vibronic origin for the $2^2\Pi-X1^2\Sigma^+$ transition was found at $18154.3~{\rm cm}^{-1}$. A rotationally resolved LIF spectrum for this band, along with a PGOPHER^{SS} generated simulation, is shown in Figure 3. The rotational structure confirmed a $^2\Pi$ excited state assignment, and the simulation used a spin—orbit coupling constant of $A_{\rm SO}=12.0~{\rm cm}^{-1}$. The upper state rotational constant, $B_0'=0.302~{\rm cm}^{-1}$, was smaller than that of the ground state, but larger than the value obtained for the $3^2\Sigma^+$ state. This indicates a smaller change in the bond length on electronic excitation and, in accord with this characteristic, only a short vibrational progression was observed for the excitation spectrum. Rotationally resolved data were obtained

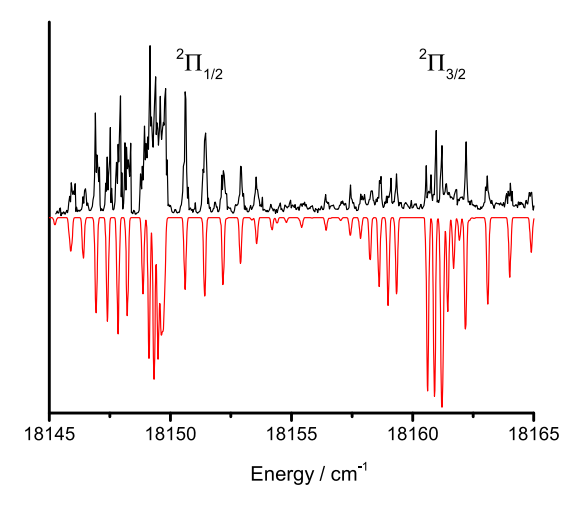


Figure 3. Origin band of the $2^2\Pi - X1^2\Sigma^+$ transition. The downward-going (red) trace is a simulation generated using the PGOPHER software package. The rotational temperature for this model was 6 K.

for the v'=0-2 vibrational levels, and the fitted molecular constants are given in Table 2. The vibrational intervals defined the constants $\omega'_e = 186.3$ and $\omega_e x'_e = 1.5$ cm⁻¹. The fluorescence decay lifetime of the $2^2\Pi$, $\nu = 0$ level, was 36 ns.

ii. Near-UV Transitions of LiMg. The near-UV bands of LiMg, first observed by Berry and Duncan⁵ using one-color RE2PI spectroscopy, were re-examined using LIF and DLIF techniques. Frequency doubling of the light from the ND6000 laser was used to generate light in the 312–333 nm wavelength range. Our results were quite similar to those of Berry and Duncan,⁵ but appeared to be consistent with a somewhat lower vibrational temperature. Partially resolved rotational structure was observed for the stronger transitions that had been assigned to the E–X and F–X transitions ($5^2\Sigma^+$ – $X1^2\Sigma^+$ and $3^2\Pi$ – $X1^2\Sigma^+$). Figure 4 shows the rotational contour for the 30383.9 cm⁻¹ band, previously assigned as the E-X 0–0 origin. On inspection, this appears to be a $2\Sigma^+$ – $2\Sigma^+$ transition with blue-shaded P- and R-branch structures. Simulations of this band, carried out using the PGOPHER software package,

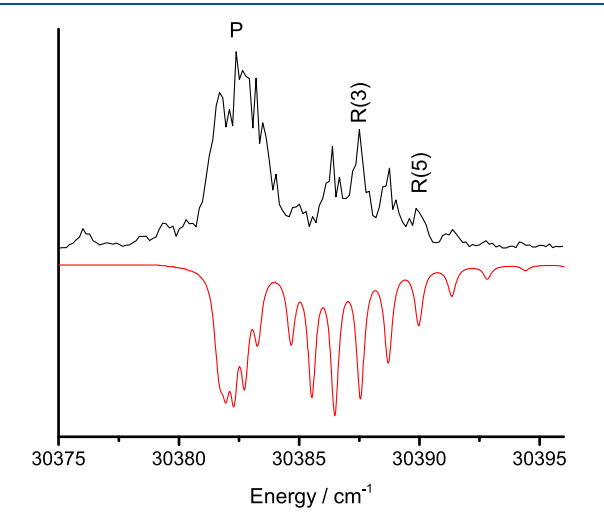


Figure 4. Rotational band contour of the transition observed at 30383 cm⁻¹. The downward-going (red) trace is a simulation generated using the PGOPHER software package. This model is for a ${}^2\Sigma^+ - {}^2\Sigma^+$ transition, with the ground state rotational constant held at $B_0'' = 0.320$ cm⁻¹. The rotational temperature for this model was 6 K.

confirmed this interpretation (cf. Figure 4). While the agreement between this noisy spectrum and the simulation is poor near the band center, models with the upper state chosen to be ${}^2\Pi$ were in obvious disagreement with the observed band contour. Surprisingly, this was the only ${}^2\Sigma^+ - {}^2\Sigma^+$ transition observed in our near-UV scans. All other bands exhibited ${}^2\Pi - {}^2\Sigma^+$ rotational contours. For example, Figure 5 shows the

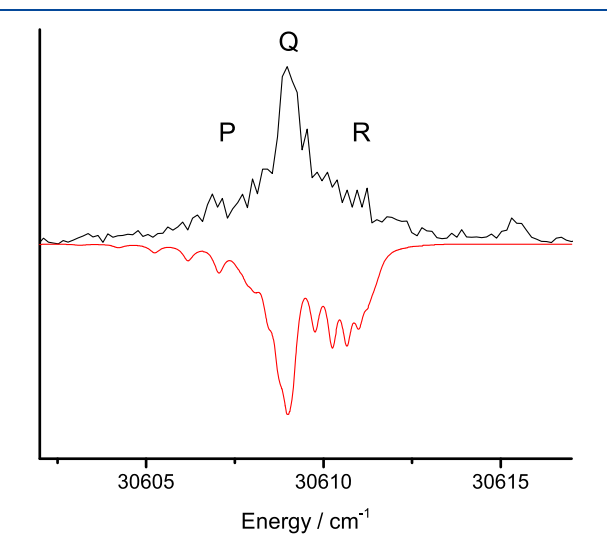


Figure 5. Rotational band contour of the transition observed at 30609 cm⁻¹. The downward-going (red) trace is a simulation generated using the PGOPHER software package. This model is for a ${}^{2}\Pi - {}^{2}\Sigma^{+}$ transition with the spin–orbit coupling constant set to zero and the ground state rotational constant held at $B_0'' = 0.320$ cm⁻¹. The rotational temperature for this model was 6 K.

rotational contour of the band at 30609.1 cm⁻¹, that was previously assigned as the E-X 1–0 band. This contour cannot be represented using a $^2\Sigma^+-^2\Sigma^+$ transition type. The simulation shown in Figure 5 is $^2\Pi-X1^2\Sigma^+$ model with the upper state spin—orbit interaction constant set to zero. Acceptable simulations were obtained provided that $A_{\rm SO}$ was kept below 1 cm⁻¹. While the rotational contours indicate that the bands at 30383.3 and 30609.1 cm⁻¹ belong to different upper electronic states, the fluorescence decay lifetimes (25 and 26 ns) did not exhibit a significant difference.

The rotational contour for a band at 31060.4 cm^{-1} is shown in Figure 6. Berry and Duncan⁵ assigned this feature as the E-X 3–0 band. Simulation of this contour indicates a $^2\Pi$ upper state with a spin–orbit interaction constant of $A_{SO} = 4.6 \text{ cm}^{-1}$ (a fluorescence decay curve was not recorded for this vibronic level).

The most intense feature of the near-UV range was a band at 31167.8 cm $^{-1}$, assigned previously as the F-X 0–0 transition. The rotational contour, presented in Figure 7, was consistent with a $^2\Pi$ upper state with a spin–orbit interaction constant of $A_{\rm SO}=7.40~{\rm cm}^{-1}$. The fluorescence decay lifetime of 52 ns was substantially longer than that of any other excited vibronic state examined in this study. The band assigned to the F-X 1–0 transition (31409.3 cm $^{-1}$) also had a $^2\Pi-{\rm X}1^2\Sigma^+$ contour, but the spin–orbit interaction constant was notably smaller ($A_{\rm SO}=4.1~{\rm cm}^{-1}$) and the fluorescence decay lifetime was shorter (27 ns). Molecular constants derived from fitting to the stronger near-UV bands of LiMg are collected in Table 4. As the upper state assignments are not established, they are labeled here using the notation $[\nu_0/1000]^{2S+1}\Lambda_\Omega$.

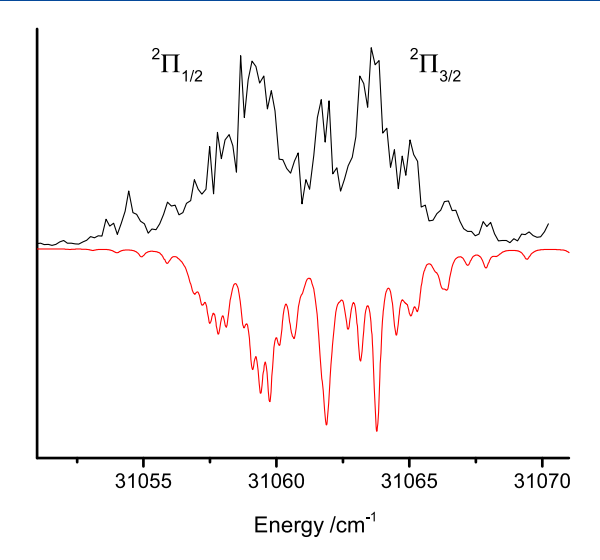


Figure 6. Rotational band contour of the transition observed at 31060 cm⁻¹. The downward-going (red) trace is a simulation generated using the PGOPHER software package. This model is for a ${}^{2}\Pi - {}^{2}\Sigma^{+}$ transition with a spin–orbit coupling constant of 4.60 cm⁻¹ and the ground state rotational constant held at $B_0'' = 0.320$ cm⁻¹. The rotational temperature for this model was 6 K.

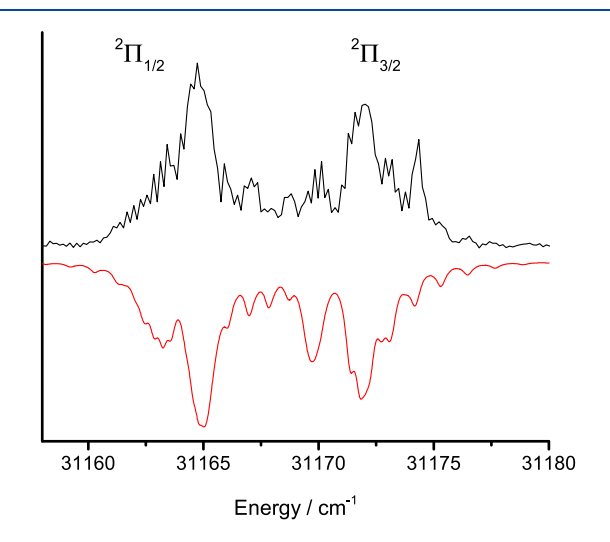


Figure 7. Rotational band contour of the transition observed at 31167 cm $^{-1}$. The downward-going (red) trace is a simulation generated using the PGOPHER software package. This model is for a $^2\Pi^{-2}\Sigma^+$ transition with a spin–orbit coupling constant of 7.40 cm $^{-1}$ and the ground state rotational constant held at $B_0^{\prime\prime}=0.320$ cm $^{-1}$. The rotational temperature for this model was 6 K.

Table 4. Molecular Constants of the Near-UV Bands of LiMg^a

excited state	ν_0	B'	A_{SO}	$ au^a$
$[30.38]^2\Sigma^+$	30383.3(1)	0.375(8)		28(1)
$[30.61]^2\Pi$	30609.1(2)	0.300(4)	<1	28(1)
$[31.06]^2\Pi$	31060.4(1)	0.344(5)	4.6(1)	
$[31.17]^2\Pi$	31167.8(1)	0.324(6)	7.6(1)	52(3)
$[31.41]^2\Pi$	31409.3(1)	0.329(12)	4.1(1)	27(4)

"Fluorescence decay lifetime in units of ns. The 1σ errors of the last digit for the molecular constants are given in parentheses.

DLIF spectra recorded using excitation of the near-UV bands provided data for the lower energy electronically excited

states. Figure 8 shows the DLIF spectrum obtained using excitation of the $[31.17]^2\Pi$ -X1² Σ ⁺ band. The vibrational

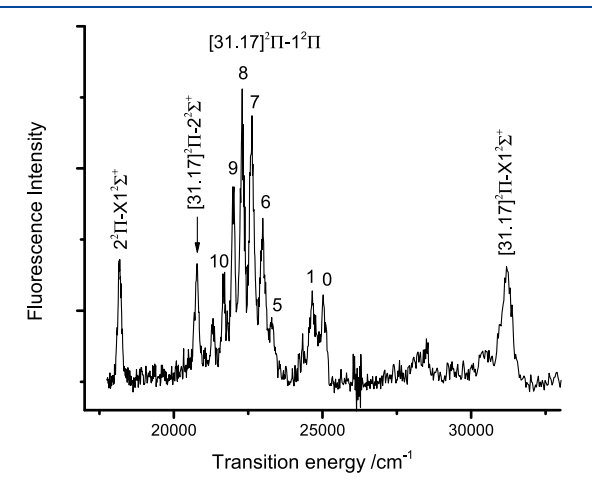


Figure 8. DLIF spectrum observed using excitation of the $[31.17]^2\Pi$ -X1² Σ ⁺ transition. See text for details.

structure of this trace in the 21250–25000 cm⁻¹ range was clearly emission down to the $1^2\Pi$ state. The origin band at 25020(30) cm⁻¹ defines a value of ν_0 = 6147(30) cm⁻¹ for the zero-point level of the $1^2\Pi$ state, reasonably close to the value of ν_0 = 6827 cm⁻¹ predicted by Gao and Gao. Fitting eq 1 to the band centers of the $[31.17]^2\Pi \rightarrow 1^2\Pi$ transition yielded lower state vibrational constants of ω_e' = 364.9(51) and $\omega_e \varkappa_e'$ = 2.66(53) cm⁻¹. The standard deviation of the fit was 13.6 cm⁻¹.

There are two other assignable features in the low energy region of Figure 8. The peak at 20780(30) cm⁻¹ was consistent with emission to the $2^2\Sigma^+$, $\nu=0$ level, defining a zero-point energy of $\nu_0=10387(30)$ cm⁻¹ (predicted¹⁰ to be 10275 cm⁻¹). The lowest energy peak at 18161(20) cm⁻¹ does not appear to be emission from $[31.17]^2\Pi$ (no suitable lower levels are predicted), but it is in agreement with the measured band origin for the $2^2\Pi$ -X1² Σ^+ transition. We propose that this band, which was present in all of the DLIF spectra excited via the near-UV bands, was excited by radiative population transfer to $2^2\Pi$.

iii. Photoionization Spectroscopy of LiMg. The IE of LiMg and the vibrational energy levels of LiMg+ were examined using two-color photoionization measurements. For these experiments the first laser pulse was tuned to excite either the 0–0 or 1–0 band of the $2^2\Pi - X1^2\Sigma^+$ transition. PIE scans were used to obtain a low-resolution estimation for the IE of 38475(20) cm⁻¹ (corrected for the local electric field using the approximation $\Delta E = 6\sqrt{F}$, where ΔE is in cm⁻¹ and F is in volts/cm). Subsequent PFI-ZEKE measurements improved the error limits for the IE and provided data for the $v^+ = 0-9$ vibrational levels of the ion. Figure 9 shows the PFI-ZEKE scan for ionization to the LiMg⁺ $X\bar{1}^1\Sigma^+$ ν^+ = 0 level. Rotational structure was not resolved for this band or for any of the higher energy vibrational states. Consequently, the band centers have been used to determine the vibrational energies. The origin band defined an IE of 38468(3) cm⁻¹. Relative energies of the vibrational states are listed in Table 3. Fitting eq 1 to these data yielded vibrational constants of ω_e^+ = 268.7(8) and $\omega_e x_e^+ = 2.47(8)$ cm⁻¹.

iv. Theoretical Calculations for LiMg. As indicated in the previous sections, published calculations for the lower

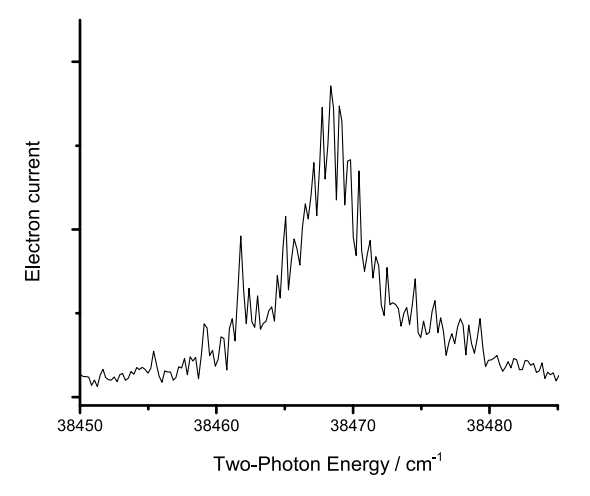


Figure 9. PFI-ZEKE spectrum of the $X1^1\Sigma^+$, v=0 level of LiMg⁺. The first laser pulse was used to excite the $2^2\Pi_{3/2}-X1^2\Sigma^+$, 0-0 $R_2(1.5)$ line at 18161 cm⁻¹.

energy states of LiMg (those correlating with the first three dissociation asymptotes of Table 1) were in reasonably good agreement with the experimental observations. At higher energies, we found that details of the near-UV bands were not in support of previous assignments. In hopes of gaining theoretical guidance for the reassignment of these bands, we carried out calculations that included all of the states listed in Table 1.

Calculations were performed at the multireference singles and doubles configuration-interaction level of theory. The Davidson correction was applied, and relativistic effects were taken into account using a third-order Douglas-Kroll model and the Breit-Pauli spin—orbit operator (denoted as MRSDCIQ-SO). The diagonal matrix elements of the spin—orbit operator were evaluated using the MRSDCI wave functions. All electronic structure calculations were carried out using the MOLPRO 2015.1 suite of programs. ⁵⁶

Our fist set of calculations were performed using the aug-cc-pwCVQZ basis sets (as provided by the MOLPRO basis set library) for both Li and Mg. The active space for the CASSCF and MRSDCI calculations consisted of the Li 2s, 2p, 3s, 3p, 3d and Mg 3s, 3p, 4s orbitals. The Li 1s and Mg 1s, 2s, and 2p orbitals were constrained to be doubly occupied, but these electrons were otherwise included in the correlation treatment. Prior to inclusion of the spin—orbit operator, energies were calculated for 24 doublet states and 13 quartet states.

Potential energy curves (PECs) were constructed by performing single-point energy calculations for a series of internuclear distances. The range was chosen to run from 2.2 to 6.8 Å in steps of 0.1 Å. Molecular constants were obtained by fitting Morse potential energy functions to the single point energies (typically 11 points in the vicinity of the equilibrium distance were used for this fitting). These calculations yielded good quality predictions for the low-energy states that correlate with the first three dissociation asymptotes of Table 1. However, PECs for the higher energy states did not show any obvious correlation with the bands observed in the near-UV spectral range. Attempts to follow the excited state PECs to their dissociation limits were prevented by the calculations being nonconvergent in the range from 4.3 to 5 Å. After some experimentation with basis sets, the problem was circumvented by using an effective core basis for the Mg atom (ECP10SDF) and the ROOS basis set for Li. This combination yielded PECs

that were in acceptable agreement with the experimental results for the lower-energy states. Higher energy states were well-behaved and extrapolated smoothly to the expected dissociation limits. This was true for both the doublet and quartet states examined in this study. To facilitate discussion of the near-UV bands, Figures 10 and 11 show the relevant PECs

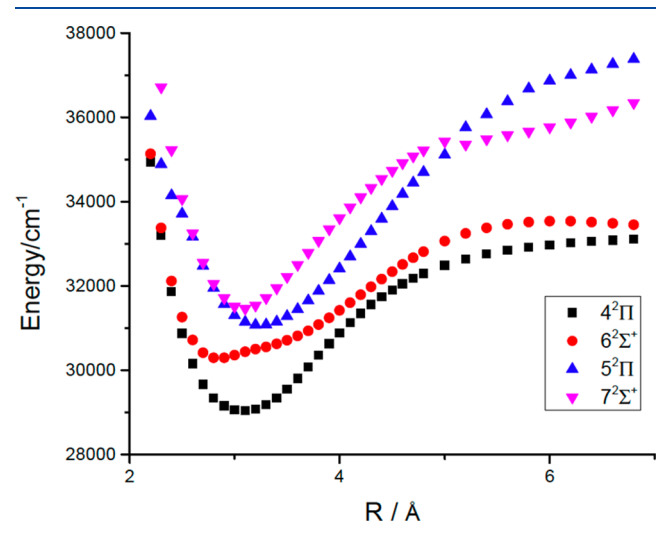


Figure 10. Computationally generated potential energy curves for excited doublet states of LiMg. Note that the spin—orbit splittings were too small to be resolved for the energy range displayed. See text for details.

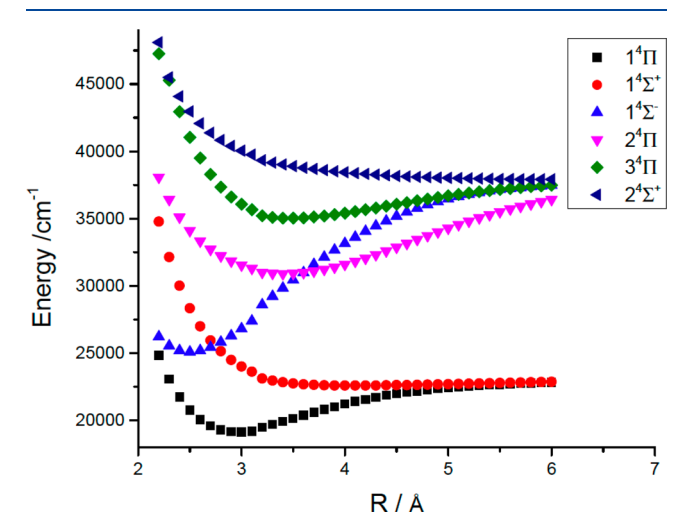


Figure 11. Computationally generated potential energy curves for excited quartet states of LiMg. Note that the spin—orbit splittings were too small to be resolved for the energy range displayed. See text for details.

for the doublet and quartet states, respectively. Calculated molecular constants for the doublet and quartet states are listed in Table 5, where we also include a subset of the results (MRCI/CVQZ+Q) from ref 10 for comparison to a calculation that considered a smaller number of excited states.

DISCUSSION

The present experimental results are in agreement with previous spectroscopic studies but provide greater detail through improved resolution. Transitions to the $1^2\Pi$ and $2^2\Sigma^+$ states are reported for the first time.

The $X1^2\Sigma^+$ ground state has been characterized through the observation of vibrational levels v'' = 0-9 and determination of the rotational constant B_0 . The vibrational intervals were well-represented by the Morse energy level expression, so it is expected that the dissociation energy obtained by means of a Birge-Sponer extrapolation ($D_c = 1424(21) \text{ cm}^{-1}$) is reasonably accurate. This result was consistent with the theoretically predicted values of 1371,3 1613,1 1435,2 1330,44 and 1379^{10} cm⁻¹. The B_0 constant establishes a vibrationally averaged R_0 bond length of 3.10 Å, which also agrees with previous theoretical calculations. It is of interest to compare the bonding in the series Li₂, LiMg, and Mg₂, where the formal bond orders are 1, 1/2, and 0, respectively. The dissociation energies, bond lengths, and harmonic vibrational constants for these molecules are collected in Table 6. These data are consistent with the expected bond orders.

In their study of LiMg chemiluminescence, Pichler et al.³⁸ observed broad, unstructured emission bands that were centered at 549 nm (18215 cm⁻¹) and 529 nm (18900 cm⁻¹). Using electronic structure calculations to guide the assignments, they proposed that the emissions corresponded to the $2^2\Pi - X1^2\Sigma^+$ and $3^2\Sigma^+ - X1^2\Sigma^+$ band systems (formerly labeled as C-X and D-X). These assignments are fully supported by the excitation and DLIF spectra reported here. As can be seen from the data in Table 5, MRCI calculations yielded molecular constants that were in reasonable agreement with the experimental results for the lower-energy states. Gao and Gao¹⁰ also reported transition dipole moments and fluorescence decay lifetimes. For the v'=0 levels of the $2^2\Pi$ and $3^2\Sigma^+$ states they obtained lifetimes of 139 and 67 ns. respectively. The measured values of 36 and 30 ns were appreciably smaller. Part of this discrepancy may be due to transitions down to the $1^2\Pi$ and $2^2\Sigma^+$ states, as these decay channels were not included in the calculations.

Assignment of the near-UV bands proved to be a more challenging problem. At the level of resolution achieved in the study by Berry and Duncan, the assignments to vibrational progressions of the E-X and F-X transitions seems entirely reasonable. However, the rotational structures of the bands do not support this interpretation.

The $[30.38]^2\Sigma^+$ level, formerly assigned as E, v' = 0, is the only ${}^2\Sigma^+$ upper level observed in this spectral range. The rotational constant indicates that the equilibrium bond length for the $[30.38]^2\Sigma^+$ state is significantly shorter than that of the $X1^2\Sigma^+$ state. Vibrational progressions were observed in the DLIF spectrum of the $[30.38]^2\Sigma^+$ state, with intensity distributions that were consistent with emission from a v' =0 level. Comparison with the theoretical results of Table 5 indicates that the upper state is $6^2\Sigma^+$, v'=0. The PEC for this state is distorted away from the usual Morse-like behavior (see Figure 10), which results in the relatively short equilibrium internuclear distance. Due to the shape of the potential, the vibration-rotation properties of this state were obtained numerically using the program Level $8.0.^{58}$ The calculated B_0 constant is slightly larger than the measured value, but the discrepancy is not exceptional. Hence, we are relatively confidant of the electronic state assignment.

The band at 30609.1 cm $^{-1}$, previously assigned 5 as E-X 1-0, has a rotational contour indicative of a $^{2}\Pi$ upper state (Figure 5) and a DLIF spectrum that shows the intensity patterns expected for emission from a v'=0 level. The electronic symmetry, DLIF and rotational constants all indicate that the bands at 30383.9 and 30609.1 cm $^{-1}$ do not belong to a

Table 5. Calculated and Measured Molecular Constants for ⁷Li²⁴Mg

state	T_e	R_e	B_e	$A_{ m SO}$	ω_e	$\omega_e x_e$	sourc
S = 1/2							
$X1^2\Sigma^+$	0	3.101	0.323		164.8	6.58	а
	0	3.103	0.323		174.2	5.89	ь
	0		$[0.320]^{c}$		187.3	6.16	expt
$1^2\Pi$	6761	2.585	0.465	14.1	357.6	2.49	а
	6732	2.606	0.457		361.1	2.67	ь
	[6147]				349.9	2.66	expt
$2^2\Sigma^+$	10546	2.940	0.359		262.7	2.00	а
	10784	2.968	0.353		256.5	2.19	ь
	[10387]						expt
$2^2\Pi$	18540	3.196	0.304	8.3	186.1	1.76	a
	18890	3.137	0.316		199.2	1.34	ь
	[18154]		[0.302]	12.0	186.3	1.50	expt
$3^2\Sigma^+$	19032	3.707	0.226		149.5	0.34	a
	19371	3.646	0.234		169.1	0.87	ь
	[19229]		[0.248]		165.4	0.82	Exp
$4^2\Sigma^+$	22908	3.016	0.341		294.6	3.42	a
$5^2\Sigma^+$	26018	2.990	0.347		211.6	2.25	а
$3^2\Pi$	26829	2.746	0.412	1.5	314.5	12.42	а
$1^2\Delta$	27018	2.795	0.389	3.8	281.1	2.91	а
$4^2\Pi$	29023	3.072	0.329	5.8	216.9	1.09	а
$6^2\Sigma^+$	30392	2.850	0.382		180.8 ^d		а
	[30383]		[0.375]				expt
5 ² Π	31072	3.240	0.296	1.4	209.0	1.02	a
$7^2\Sigma^+$	31490	3.073	0.327		263.2	2.39	а
5 ² Π	33527	3.171	0.309	10.9	189.3	2.91	а
S = 3/2							
$1^4\Pi$	19167	2.935	0.361	7.4	255.9	3.56	а
	19619	2.987	0.348		240.2	3.36	ь
$1^4\Sigma^-$	25087	2.497	0.489		354.7	2.04	а
$2^4\Pi$	30904	3.430	0.264		184.1	0.59	а
$3^4\Pi$	35008	3.498	0.254		177.1	2.75	а

[&]quot;Present calculations. All values are in cm⁻¹, other than R_e in Å. "MRCI/CVQZ+Q results from ref 10. "Square brackets indicate measured T_0 and B_0 values. "This is the $\Delta G_{1/2}$ value computed using the program level 8.0.⁵⁸

Table 6. Comparison of the Ground State Spectroscopic Constants of Li₂, LiMg, and Mg₂^a

	$^{7}\mathrm{Li}_{2}$	$^{7}\mathrm{Li^{24}Mg}$	$^{24}Mg_2$
$\omega_e \; (\mathrm{cm}^{-1})$	351.4	187.3	51.5
R_e (Å)	2.67	3.10 ^a	3.89
D_e (cm ⁻¹)	8517	1424	399
source	59	this study	60

^aThis is the R_0 value estimated using B_0 .

common upper electronic state. The theoretical predictions offer $S^2\Pi$ and $2^4\Pi$ as plausible assignments for the $[30.61]^2\Pi$ state. The fit to the term energy is clearly better for the assignment to $2^4\Pi$, but the discrepancy for the assignment to $S^2\Pi$ (463 cm $^{-1}$) is still within an acceptable range. The comparison of the rotational constants and the short fluorescence decay lifetime both favor the assignment to $S^2\Pi$.

If the above assignment to $5^2\Pi \text{ v}' = 0$ is adopted, the choices for assignment of $[31.06]^2\Pi$ are limited. Berry and Duncan⁵ had assigned this transition as the E-X 3–0 band. As we now know that the band assigned as the E-X origin belongs to a different electronic state, it seems reasonable to renumber the vibrational progression (such that the band seen by Berry and Duncan at 30831.4 cm⁻¹ is assigned to the $5^2\Pi - \text{X}1^2\Sigma^+$ 1–0 transition). However, there are significant problems for this

scheme. The rotational constant for the putative v'=2 level is larger than that of the v'=0 level, and the spin—orbit coupling constants for $[30.61]^2\Pi$ and $[31.06]^2\Pi$ are significantly different, indicating that they do not belong to a common electronic state. As an alternative, the band at 31060.4 cm $^{-1}$ is close to the predicted energy of the $2^4\Pi$ state. The problem with this assignment is that the transition would be spin-forbidden, but it appears with an intensity that is comparable to that of the allowed transitions in this energy range. Unfortunately, DLIF and fluorescence decay lifetime data were not collected for this upper level.

The 31167.3 cm⁻¹ band, previously assigned⁵ to the F-X 0–0 transition, exhibited a $^2\Pi$ upper state with a spin–orbit interaction constant of $A_{SO}=7.6~{\rm cm}^{-1}$. The DLIF spectrum for this upper state (Figure 8) had intensity contours that indicate an upper state level that has some degree of vibrational excitation. This level may be perturbed as it exhibited a lifetime that was significantly greater than that of any other level observed in this study. The predicted PECs for the quartet states (Figure 11) indicate that mixing with the $2^4\Pi$ state could be involved. Comparing the properties of the $[31.17]^2\Pi$ state with the theoretical results from Table 5, assignment to $6^2\Pi$ is plausible and supported by the prediction of the spin–orbit coupling constant. However, the error in the predicted term energy of 2359 cm⁻¹ is rather large.

The band at 31409.3 cm⁻¹, previously assigned to the F-X 1–0 transition,⁵ presents further difficulties. The upper state rotational constant is slightly larger than that of the $[31.17]^2\Pi$ state and the spin–orbit interaction constant and the fluorescence decay lifetime are smaller by factors close to 2. The DLIF spectrum shows vibrational intensity patterns that indicate emission from v'=0. There is no obvious match with the states predicted by the theoretical calculations. In future studies, guidance from calculations performed with an active space that includes the Mg 3d orbitals will be needed to explain the fragmentary nature of the near-UV range spectrum.

PFI-ZEKE measurements established an IE for LiMg of $38468(3) \text{ cm}^{-1} (4.7695(4) \text{ eV})$. This value confirms that the mass spectrometric result⁷ of 5.96 eV was in error by 1.19 eV, as noted in previous theoretical studies.^{2,5} Few experimental details were provided in ref 7, so we were not able to discern the cause of the large discrepancy. For direct comparison to theoretical calculations, the adiabatic IE (IE_{ad}), obtained by removing the vibrational zero-point energies from the measured IE, was 38443(20) cm⁻¹. Gao and Gao¹⁰ did not report a value for IE_{ad}, but this can be determined from the ground state dissociation energies for LiMg and LiMg+, and the accurately known IE for Li (43487.114 cm⁻¹).⁵⁷ Their MRCI/CVQZ+Q calculations yield $IE_{ad} = 38403$ cm⁻¹, in excellent agreement with the measured value. Boldyrev et al.² also obtained close agreement, reporting a value of IE_{2d} = 37990 cm⁻¹. The molecular IE being less than that of atomic Li directly reflects the greater bond dissociation energy of the molecular cation $(D_0^+ - D_0 = 5020 \text{ cm}^{-1})$. This is readily anticipated as ionization removes an electron from the $6\sigma^*$ antibonding orbital. Computed values for the harmonic vibrational constant of LiMg⁺ also proved to be close to the experimental result of 268.7(8) cm⁻¹. Values for ω_e^+ of 263.5, 264.2, and 261 cm⁻¹ were reported in refs 2, 10, and 16, respectively. Consistent with the increase in the bond strength, theoretical calculations indicate that the equilibrium distance contracts on ionization. Calculated values of $R_e^+ = 2.935$ and 2.89 Å are reported in refs 1, 2, and 16.

SUMMARY

Electronic spectroscopy has been used to characterize the $X1^2\Sigma^+$, $1^2\Pi$, $2^2\Sigma^+$, $2^2\Pi$, and $3^2\Sigma^+$ states of LiMg. Rotational resolution was achieved for bands of the $2^2\Pi-X1^2\Sigma^+$ and $3^2\Sigma^+-X1^2\Sigma^+$ transitions, providing the first data for the ground state rotational constant. Dispersed fluorescence measurements were used to observe ground state vibrational levels up to $\mathbf{v}''=9$, allowing for an improved determination of the bond dissociation energy. The ground state molecular constants were consistent with a half-order bond, and the properties of the low-energy excited states were in good agreement with high-level computational predictions. Vibrational constants for the $1^2\Pi$ state were also determined from DLIF data.

Bands that had been previously observed in the near-UV spectral range $(30300-31500~\text{cm}^{-1})^5$ were re-examined. These features had been assigned to vibrational progressions of the $3^2\Pi-X1^2\Sigma^+$ and $5^2\Sigma^+-X1^2\Sigma^+$ transitions, but the partially resolved rotational contours were not consistent with these assignments. New multireference configuration interaction calculations were carried out to explore the most probable state assignments. The results were used to identify the lowest energy feature as the $6^2\Sigma^+-X1^2\Sigma^+$ 0–0 transition. Tentative assignments were discussed for the remaining near-UV bands.

The IE for LiMg and the vibrational energy levels of LiMg⁺ $\rm X1^1\Sigma^+$ were examined by means of two-photon ionization spectroscopy. The IE (4.7695(4) eV) confirmed previous theoretical estimates^{2,10} and was in conflict with the only published experimental value of 5.96(0.01) eV.⁷ The vibrational constants and bond dissociation energy for LiMg⁺ indicated a substantial increase in the bond strength on ionization, in agreement with the expected removal of the electron from the $6\sigma^*$ antibonding orbital.

AUTHOR INFORMATION

Corresponding Author

Michael C. Heaven — Department of Chemistry, Emory University, Atlanta, Georgia 30322, United States; orcid.org/0000-0003-4738-2408; Phone: (404) 727 6617; Email: heaven@euch4e.chem.emory.edu

Authors

Thomas D. Persinger – Department of Chemistry, Emory University, Atlanta, Georgia 30322, United States Jiande Han – Department of Chemistry, Emory University, Atlanta, Georgia 30322, United States

Complete contact information is available at: https://pubs.acs.org/10.1021/acs.jpca.1c01656

Notes

I

The authors declare no competing financial interest.

ACKNOWLEDGMENTS

We are most grateful to Prof. Michael D. Morse for his careful reading of this paper and insightful comments concerning the electronic structure of LiMg. This work was supported by the National Science Foundation under Grant CHE-1900555.

REFERENCES

- (1) Bauschlicher, C. W., Jr.; Langhoff, S. R.; Partridge, H. Theoretical study of the beryllium-lithium, beryllium-sodium, magnesium-lithium, magnesium-sodium, and aluminum-beryllium (BeLi, BeNa, MgLi, MgNa, and AlBe) molecules and their negative ions. *J. Chem. Phys.* **1992**, *96*, 1240–7.
- (2) Boldyrev, A. I.; Simons, J.; Schleyer, P. v. R. Ab initio study of the electronic structures of lithium containing diatomic molecules and ions. *J. Chem. Phys.* **1993**, *99*, 8793–504.
- (3) Jones, R. O. Molecular bonding in lithium-beryllium (LiBe), lithium-magnesium (LiMg), and lithium-calcium (LiCa). *J. Chem. Phys.* **1980**, 72, 3197–200.
- (4) Schlachta, R.; Fischer, I.; Rosmus, P.; Bondybey, V. E. The simplest heteronuclear metal cluster lithium-beryllium (LiBe). *Chem. Phys. Lett.* **1990**, *170*, 485–91.
- (5) Berry, K. R.; Duncan, M. A. Photoionization spectroscopy of LiMg. Chem. Phys. Lett. 1997, 279, 44-49.
- (6) Russon, L. M.; Rothschopf, G. K.; Morse, M. D.; Boldyrev, A. I.; Simons, J. Two-photon ionization spectroscopy and all-electron ab initio study of LiCa. *J. Chem. Phys.* **1998**, *109*, 6655–6665.
- (7) Wu, C. H.; Ihle, H. R. Atomization energies and heats of formation of the molecules magnesium lithium (MgLi and Mg₂Li₂). *Adv. Mass Spectrom.* **1980**, *8A*, 374–7.
- (8) Kotochigova, S.; Petrov, A.; Linnik, M.; Klos, J.; Julienne, P. S. Ab initio properties of Li-group-II molecules for ultracold matter studies. *J. Chem. Phys.* **2011**, *135*, 164108.
- (9) Augustovicova, L.; Soldan, P. Ab initio properties of MgAlk (Alk = Li, Na, K, Rb, Cs). *J. Chem. Phys.* **2012**, *136*, 084311.
- (10) Gao, Y.; Gao, T. Ab initio study of ground and low-lying excited states of MgLi and MgLi⁺ molecules with valence full

- configuration interaction and MRCI method. *Mol. Phys.* **2014**, *112*, 3015–3023.
- (11) Gopakumar, G.; Abe, M.; Kajita, M.; Hada, M. Ab initio study of permanent electric dipole moment and radiative lifetimes of alkaline-earth-metal–Li molecules. *Phys. Rev. A: At., Mol., Opt. Phys.* **2011**, *84*, 062514.
- (12) You, Y.; Yang, C.-L.; Wang, M.-S.; Ma, X.-G.; Liu, W.-W. Theoretical investigation of the laser cooling of a LiBe molecule. *Phys. Rev. A: At., Mol., Opt. Phys.* **2015**, 92 (3-A), 032502.
- (13) Lackner, F.; Krois, G.; Buchsteiner, T.; Pototschnig, J. V.; Ernst, W. E. Helium-droplet-assisted preparation of cold RbSr molecules. *Phys. Rev. Lett.* **2014**, *113*, 153001.
- (14) Pototschnig, J. V.; Krois, G.; Lackner, F.; Ernst, W. E. Investigation of the RbCa molecule: Experiment and theory. *J. Mol. Spectrosc.* **2015**, *310*, 126–134.
- (15) Pototschnig, J. V.; Meyer, R.; Hauser, A. W.; Ernst, W. E. Vibronic transitions in the alkali-metal (Li, Na, K, Rb) alkaline-earth-metal (Ca, Sr) series: a systematic analysis of de-excitation mechanisms based on the graphical mapping of Frank-Condon integrals. *Phys. Rev. A: At., Mol., Opt. Phys.* **2017**, *95*, 022501.
- (16) ElOualhazi, R.; Berriche, H. Electronic structure and spectra of the MgLi⁺ ionic molecule. *J. Phys. Chem. A* **2016**, *120*, 452–465.
- (17) Ghanmi, C.; Farjallah, M.; Berriche, H. Theoretical study of the alkaline-earth (LiBe)⁺ ion: structure, spectroscopy and dipole moments. *J. Phys. B: At., Mol. Opt. Phys.* **2017**, *50* (5), 055101.
- (18) Bala, R.; Nataraj, H. S.; Abe, M.; Kajita, M. Accurate ab initio calculations of spectroscopic constants and properties of BeLi⁺. *J. Mol. Spectrosc.* **2018**, 349, 1–9.
- (19) Farjallah, M.; Ghanmi, C.; Berriche, H.; Al-Hajry, A.; Umar, A.; Al-Harbi, H.; Bouarissa, N.; Berriche, H.; El-Ghazaly, M. Theoretical study of the low-lying $^1\Sigma^+$ electronic states of the alkaline earth BeLi⁺ ion. *AIP Conf. Proc.* **2010**, *1370*, 215–220.
- (20) Farjallah, M.; Sardar, D.; El-Kork, N.; Deb, B.; Berriche, H. Electronic structure and photoassociation scheme of ultracold (MgK⁺) molecular ions. *J. Phys. B: At., Mol. Opt. Phys.* **2019**, *52*, 045201.
- (21) Fischer, I.; Bondybey, V. E.; Rosmus, P.; Werner, H. J. Theoretical study of the electronic states of beryllium lithium and beryllium dimer ion(1+). *Chem. Phys.* **1991**, *151*, 295–308.
- (22) Farjallah, M.; El-Korek, N.; Korek, M.; Berriche, H. Theoretical study of MgNa⁺ ionic system: potential energy curve, vibrational levels, dipole moments, radiative lifetimes and laser-cooling analysis. *Eur. Phys. J. D* **2020**, *74*, 234.
- (23) Ladjimi, H.; Farjallah, M.; Berriche, H. Spectroscopic, structural and lifetime calculations of the ground and low-lying excited states of the BeNa⁺, BeK⁺, and BeRb⁺ molecular ions. *Phys. Scr.* **2020**, *95*, 055404.
- (24) Zrafi, W.; Ladjimi, H.; Said, H.; Berriche, H.; Tomza, M. Ab initio electronic structure and prospects for the formation of ultracold calcium-alkali-metal-atom molecular ions. *New J. Phys.* **2020**, 22, 073015.
- (25) Allouche, A. R.; Aubert-Frecon, M. Theoretical study of the low-lying electronic states of the CaLi molecule. *Chem. Phys. Lett.* **1994**, 222, 524–8.
- (26) Allouche, A. R.; Aubert-Frecon, M. Electronic structure of BaLi. I. Theoretical study. *J. Chem. Phys.* **1994**, *100*, 938–44.
- (27) Benard, D. J.; Slafer, W. D. Laser induced fluorescence spectra of potassium-magnesium (KMg). *Chem. Phys. Lett.* **1978**, *56*, 438–42.
- (28) Chmaisani, W.; El-Kork, N.; Korek, M. Theoretical electronic structure of the NaBe molecule. *Chem. Phys.* **2017**, 491, 33–41.
- (29) D'Incan, J.; Effantin, C.; Bernard, A.; Fabre, G.; Stringat, R.; Boulezhar, A.; Verges, J. Electronic structure of BaLi. II. First observation of the Ba^{6,7}Li spectrum: analysis of the (2)²>-X²>+ system. *J. Chem. Phys.* **1994**, *100*, 945–9.
- (30) Guerout, R.; Aymar, M.; Dulieu, O. Ground state of the polar alkali-metal-atom-strontium molecules: Potential energy curve and permanent dipole moment. *Phys. Rev. A: At., Mol., Opt. Phys.* **2010**, 82 (4), 042508.

- (31) Ivanova, M.; Stein, A.; Pashov, A.; Stolyarov, A. V.; Knoeckel, H.; Tiemann, E. The X²>⁺ state of LiCa studied by Fourier-transform spectroscopy. *J. Chem. Phys.* **2011**, *135*, 174303.
- (32) Ladjimi, H.; Farjallah, M.; Mlika, R.; Allouche, A. R.; Berriche, H. Ab initio calculations of electronic structure of the BaCs molecule: adiabatic potential energy curves, spectroscopic constants, spin-orbit effect and permanent and transition electric dipole moments. *Theor. Chem. Acc.* **2019**, *138*, 1–17.
- (33) Ladjimi, H.; Zrafi, W.; Allouche, A.-R.; Berriche, H. Ab-initio study of the ground and low-lying excited states including the spin-orbit effect of RbBa molecule and laser cooling feasibility. *J. Quant. Spectrosc. Radiat. Transfer* **2020**, 252, 107069.
- (34) Li, S.; Wan, M.-J.; Chen, S.-J.; Jin, Y.-Y.; Zhang, C.-Z.; Chen, P.; Wang, N. An ab initio investigation on the low-lying electronic states of NaMg. *Spectrochim. Acta, Part A* **2018**, 202, 368–375.
- (35) Neumann, D. K.; Benard, D. J. Formation and decay kinetics of optically pumped lithium-magnesium excimers. *Chem. Phys. Lett.* **1982**, *88*, 429–33.
- (36) Neumann, D. K.; Benard, D. J.; Michels, H. H. Laser chemiluminescence of lithium-calcium (LiCa). *Chem. Phys. Lett.* **1980**, 73, 343–7.
- (37) Pak, K.; Ermler, W. C.; Kern, C. W.; Bondybey, V. E. Full spin-orbit configuration interaction calculations on electronic states of lithium-beryllium (LiBe). *J. Cluster Sci.* **1991**, *2*, 19–28.
- (38) Pichler, G.; Lyyra, A. M.; Kleiber, P. D.; Stwalley, W. C.; Hammer, R.; Sando, K. M.; Michels, H. H. Laser-induced chemiluminescence of the lithium-magnesium (LiMg) excimer. *Chem. Phys. Lett.* **1989**, *156*, 467–71.
- (39) Pototschnig, J. V.; Hauser, A. W.; Ernst, W. E. Electric dipole moments and chemical bonding of diatomic alkali-alkaline earth molecules. *Phys. Chem. Chem. Phys.* **2016**, *18*, 5964–5973.
- (40) Stringat, R.; Fabre, G.; Boulezhar, A.; Dincan, J.; Effantin, C.; Verges, J.; Bernard, A. The $X^{2>+}$, $(2)^{2>+}$, and $(2)^{2>}$ states of BaLi. *J. Mol. Spectrosc.* **1994**, *168*, 514–21.
- (41) Verges, J.; d'Incan, J.; Effantin, C.; Bernard, A.; Fabre, G.; Stringat, R.; Boulezhar, A. Electronic structure of BaLi: the (2)²>+ state. *J. Phys. B: At., Mol. Opt. Phys.* **1994**, 27, L153–L155.
- (42) Benard, D. J.; Michels, H. H. Laser-induced chemiluminescence of sodium-magnesium. *Chem. Phys. Lett.* **1982**, *86*, 449–52.
- (43) Ciamei, A.; Szczepkowski, J.; Bayerle, A.; Barbe, V.; Reichsoellner, L.; Tzanova, S. M.; Chen, C.-C.; Pasquiou, B.; Grochola, A.; Kowalczyk, P.; et al. The RbSr $^2\Sigma^+$ ground state investigated via spectroscopy of hot and ultracold molecules. *Phys. Chem. Chem. Phys.* **2018**, *20*, 26221–26240.
- (44) Gopakumar, G.; Abe, M.; Hada, M.; Kajita, M. Dipole polarizability of alkali-metal (Na, K, Rb)-alkaline-earth-metal (Ca, Sr) polar molecules: Prospects for alignment. *J. Chem. Phys.* **2014**, *140*, 224303.
- (45) Krois, G.; Lackner, F.; Pototschnig, J. V.; Buchsteiner, T.; Ernst, W. E. Characterization of RbSr molecules: spectral analysis on helium droplets. *Phys. Chem. Chem. Phys.* **2014**, *16*, 22373–22381.
- (46) Zuchowski, P. S.; Aldegunde, J.; Hutson, J. M. Ultracold RbSr molecules can be formed by magnetoassociation. *Phys. Rev. Lett.* **2010**, 105, 153201.
- (47) Ivanova, M.; Stein, A.; Pashov, A.; Stolyarov, A. V.; Knoeckel, H.; Tiemann, E. The $X^2\Sigma^+$ state of LiCa studied by Fourier-transform spectroscopy. *J. Chem. Phys.* **2011**, *135*, 174303.
- (48) Stein, A.; Ivanova, M.; Pashov, A.; Knoeckel, H.; Tiemann, E. Spectroscopic study of the $2^2\Sigma^+$ and the $4^2\Sigma^+$ excited states of LiCa. *J. Chem. Phys.* **2013**, *138*, 114306.
- (49) Schwanke, E.; Gerschmann, J.; Knoeckel, H.; Ospelkaus, S.; Tiemann, E. The coupled system $(2)^2\Sigma^+$ and $(1)^2\Pi$ of $^7Li^{88}$ Sr. *J. Phys. B: At., Mol. Opt. Phys.* **2020**, *53*, 065102.
- (50) Schwanke, E.; Knoeckel, H.; Stein, A.; Pashov, A.; Ospelkaus, S.; Tiemann, E. Laser and Fourier transform spectroscopy of ⁷Li⁸⁸Sr. *J. Phys. B: At., Mol. Opt. Phys.* **2017**, *50*, 235103.
- (51) Antonov, I. O.; Barker, B. J.; Bondybey, V. E.; Heaven, M. C. Spectroscopic characterization of $Be_2^+X^{2>+}$ and the ionization energy of Be_2 . *J. Chem. Phys.* **2010**, *133*, 074309.

- (52) Fedorov, D. A.; Barnes, D. K.; Varganov, S. A. Ab initio calculations of spectroscopic constants and vibrational state lifetimes of diatomic alkali-alkaline-earth cations. *J. Chem. Phys.* **2017**, *147*, 124304.
- (53) Duncan, M. A. Laser vaporization cluster sources. Rev. Sci. Instrum. 2012, 83, 041101.
- (54) Heaven, M. C. Probing actinide electronic structure using fluorescence and multi-photon ionization spectroscopy. *Phys. Chem. Chem. Phys.* **2006**, *8*, 4497–4509.
- (55) Western, C. M. PGOPHER: A program for simulating rotational, vibrational and electronic spectra. *J. Quant. Spectrosc. Radiat. Transfer* **2017**, *186*, 221–242.
- (56) Werner, H.-J.; Knowles, P. J.; Knizia, G.; Manby, F. R.; Schuetz, M. Molpro: a general-purpose quantum chemistry program package. *Wiley Interdiscip. Rev. Comput. Mol. Sci.* **2012**, *2*, 242–253.
- (57) NIST Atomic Spectra Database (ver. 5.8), https://physics.nist.gov/asd.
- (58) Le Roy, R. J. LEVEL: A computer program for solving the radial Schrodinger equation for bound and quasibound levels. *J. Quant. Spectrosc. Radiat. Transfer* **2017**, *186*, 167–178.
- (59) Coxon, J. A.; Melville, T. C. Application of direct potential fitting to line position data for the $X^1\Sigma_g^+$ and $A^1\Sigma_u^+$ states of Li₂. *J. Mol. Spectrosc.* **2006**, 235, 235–247.
- (60) Balfour, W. J.; Douglas, A. E. Absorption spectrum of the diatomic magnesium molecule. *Can. J. Phys.* **1970**, *48*, 901–14.